BIOLOGY OF REPRODUCTION 70, 1428–1437 (2004)
Published online before print 21 January 2004.
DOI 10.1095/biolreprod.103.025296

Variation in the Membrane Transport Properties and Predicted Optimal Rates of Freezing for Spermatozoa of Diploid and Tetraploid Pacific Oyster, *Crassostrea gigas*[1]

Yimeng He,[3] Qiaoxiang Dong,[4] Terrence R. Tiersch,[4] and Ram V. Devireddy[2,3]

Bioengineering Laboratory,[3] Department of Mechanical Engineering, Louisiana State University, Baton Rouge, Louisiana 70803
Aquaculture Research Station,[4] Louisiana Agricultural Experiment Station, Louisiana State University Agricultural Center, Baton Rouge, Louisiana

ABSTRACT

In the present study, a shape-independent differential scanning calorimeter (DSC) technique was used to measure the dehydration response during freezing of sperm cells from diploid and tetraploid Pacific oysters, *Crassostrea gigas*. This represents the first application of the DSC technique to sperm cells from nonmammalian species. Volumetric shrinkage during freezing of oyster sperm cell suspensions was obtained at cooling rates of 5 and 20°C/min in the presence of extracellular ice and 8% (v/v) concentration of dimethyl sulfoxide (DMSO), a commonly used cryoprotective agent (CPA). Using previously published data, sperm cells from diploid oysters were modeled as a two-compartment "ball-on-stick" model with a "ball" 1.66 μm in diameter and a "stick" 41 μm in length and 0.14 μm wide. Similarly, sperm cells of tetraploid oysters were modeled with a "ball" 2.14 μm in diameter and a "stick" 53 μm in length and 0.17 μm wide. Sperm cells of both ploidy levels were assumed to have an osmotically inactive cell volume, V_b, of 0.6 V_o, where V_o is the isotonic (or initial) cell volume. By fitting a model of water transport to the experimentally obtained volumetric shrinkage data, the best-fit membrane permeability parameters (L_{pg} and E_{Lp}) were determined. The combined-best-fit membrane permeability parameters at 5 and 20°C/min for haploid sperm cells (or cells from diploid Pacific oysters) in the absence of CPAs were: $L_{pg} = 0.30 \times 10^{-15}$ m³/Ns (0.0017 μm/min-atm) and $E_{Lp} = 41.0$ kJ/mole (9.8 kcal/mole). The corresponding parameters in the presence of 8% DMSO were: $L_{pg}[cpa] = 0.27 \times 10^{-15}$ m³/Ns (0.0015 μm/min-atm) and $E_{Lp}[cpa] = 38.0$ kJ/mole (9.1 kcal/mole). Similarly, the combined-best-fit membrane permeability parameters at 5 and 20°C/min for diploid sperm cells (or cells from tetraploid Pacific oysters) in the absence of CPAs were: $L_{pg} = 0.34 \times 10^{-15}$ m³/Ns (0.0019 μm/min-atm) and $E_{Lp} = 29.7$ kJ/mole (7.1 kcal/mole). The corresponding parameters in the presence of 8% DMSO were: $L_{pg}[cpa] = 0.34 \times 10^{-15}$ m³/Ns (0.0019 μm/min-atm) and $E_{Lp}[cpa] = 37.6$ kJ/mole (9.0 kcal/mole). The parameters obtained in this study suggest that optimal rates of cooling for Pacific oyster sperm cells range from 40 to 70°C/min. These theoretical cooling rates are in close conformity with empirically determined optimal rates of cooling sperm cells from Pacific oysters, *C. gigas*.

gamete biology, sperm, sperm motility and transport

INTRODUCTION

During freezing of any cell suspension, ice nucleates initially in the extracellular space causing an osmotic gradient to be set up across the intracellular isotonic solution and the freeze-concentrated extracellular solution [1, 2]. Depending on the cooling rate, the intracellular water permeates across the cell membrane and joins the extracellular ice phase or freezes and forms ice inside the cell. In most cases, cells undergoing ice formation inside the cells or intracellular ice formation (IIF) are rendered osmotically inactive (lysed) because of the loss of cell membrane integrity [3]. Similarly cells that experience a severe loss of intracellular water and the associated long-term exposure to the highly concentrated extracellular salt solutions are also rendered osmotically inactive [4]. Both IIF and long exposures to high solute concentrations are lethal to cells. So cooling rates that are either too slow or too fast can kill cells; therefore, an optimal cooling rate should exist between slow and fast rates. This has been confirmed experimentally for a variety of cells, and the curve of cell survival plotted as a function of the cooling rate has a characteristic inverted U shape [5]. Whether a prescribed cooling rate is too slow or fast is a function of cell membrane permeability to water and the probability that any water remaining trapped within the cell at any given subzero temperature will nucleate and turn to ice. Differences in membrane permeability to water and the probability of IIF result in different optimal cooling rates for different cells. Therefore, to optimize a cryopreservation protocol, it is important to measure the cell membrane permeability to water.

Cryopreservation has been studied in aquatic species for more than 50 yr [6–8]; however, with some notable exceptions [e.g., 9–11], cryobiology has largely been neglected in these species. Most research in the 200 or so species that have been studied has addressed empirical development of basic cryopreservation procedures [12–14]. Similarly, without firm cryobiology understanding, sperm cryopreservation of diploid oysters has been studied in several species, predominantly the Pacific oyster *Crassostrea gigas* [e.g., 15–19], the eastern oyster, *C. virginica* [20–22], and others [23]. Because reduced gonadal development is associated with improved meat quality and growth [24, 25], triploid oysters (with three sets of chromosomes), which are functionally sterile, offer advantages over diploid oysters. Com-

[1]Supported in part by funding from the Louisiana Board of Regents (LEQSF 2002-05-RD-A-03) and the USDA-SBIR program. This manuscript was approved for publication by the Director of the Louisiana Agricultural Experiment Station as manuscript 03-11-1573.
[2]Correspondence: Ram Devireddy, Department of Mechanical Engineering, Louisiana State University, Baton Rouge, LA 70803. FAX: 225 578 5924; e-mail: devireddy@me.lsu.edu

Received: 13 November 2003.
First decision: 5 December 2003.
Accepted: 9 January 2004.

ISSN: 0006-3363. http://www.biolreprod.org

mercial application of triploid oysters requires efficient methods for triploidy production such as crossing of diploids with tetraploids (that possess four sets of chromosomes), which in turn requires the availability of tetraploid oysters in the hatchery [26]. Clearly, sperm cryopreservation of tetraploid oysters can be a critical tool for commercial-scale application of tetraploid stocks and the consequent expansion of the worldwide triploid oyster market.

Further usage of thawed oyster sperm requires a firm biophysical understanding of the cryopreservation process. Currently the bulk of our understanding in the cryopreservation of oyster sperm (as well as in other aquatic and mammalian species) is still empirical in nature. Because the unique size and morphology of sperm cells limits the applicability of standard cellular cryomicroscopy techniques to measure the biophysical response (water transport and intracellular ice formation) during a freezing process. However, a recent advance in measurement methodology, namely a differential scanning calorimetry (DSC)-based technique [27], has improved our knowledge of the water transport response during freezing in several mammalian gametes, including mouse [28], human [29], horse [30], canine [31], and boar [32]. The DSC technique will also be used, for the first time with an aquatic species, in the present study to improve our understanding of the biophysical response during freezing of sperm cells from diploid and tetraploid Pacific oysters.

The aim of this project was to establish the membrane permeability parameters of sperm cells of diploid and tetraploid Pacific oysters, *C. gigas*. In the DSC technique, two heat releases from the same cell suspension are measured: 1) during freezing of osmotically active (live) cells in media (in which the intracellular water is being transported across the membrane to freeze in the extracellular space) and 2) during freezing of osmotically inactive (dead) cells in media. The difference in heat release measured between the two cooling trials is correlated to water transport (see a recent review by Devireddy and Bischof [33] and has been independently verified by Yuan and Diller [34] and Diller [35]. The experimentally determined parameters for Pacific oyster sperm membrane permeability were used to numerically predict the loss of intracellular water at various cooling rates (5–100°C/min). And finally, the numerical models were analyzed to predict the amount of water left in the sperm cell after dehydration ceases, in the absence of IIF, and to predict optimal cooling rates for Pacific oyster sperm cryopreservation.

MATERIALS AND METHODS

Collection and Isolation of Sperm Cells

Tetraploid and diploid Pacific oysters were obtained in August 2003 from the Taylor Resources Quilcene Shellfish Hatchery (Quilcene, WA) and were shipped chilled by overnight delivery to the Louisiana State University (LSU) Agricultural Center, Aquaculture Research Station (ARS). Sperm were collected by dry stripping of the gonad [26] and suspended in calcium-free Hanks balanced salt solution at 1000 mOsmol/kg [20]. Sperm concentrations were adjusted to 1–2 × 10^9 cells/ml. The sample was transported to the LSU bioengineering laboratory for DSC experiments.

DSC Experiments

The DSC dynamic cooling experiments were performed on concentrated oyster sperm samples in standard aluminum sample pans (Perkin Elmer Corporation, Norwalk, CT). The concentration of the sperm suspension used in the DSC experiments ranged from 1 to 2 × 10^9 cells/ml. Approximately 10 μl of this sperm suspension was loaded in a DSC sample pan. The DSC dynamic cooling protocol used to measure the water transport out of Pacific oyster sperm cells is the same as reported in earlier studies on mammalian cells [27–33] and will be only briefly stated here.

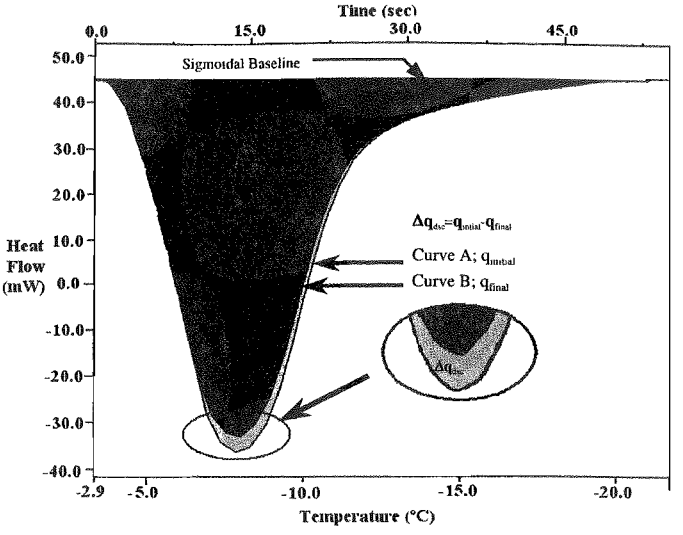

FIG. 1. Superimposed heat flow thermograms obtained during the initial (live cells; curve A) and final (dead cells; curve B) cooling trials for diploid sperm cells (or cells from tetraploid Pacific oysters) at a cooling rate of 20°C/min obtained in the presence of DMSO. The negative values on the y-axis for the heat flow imply an exothermic heat release in the DSC sample. The heat flow (mW/mg) is plotted along the y-axis and the subzero temperatures (°C) are plotted along the top x-axis and time (sec) is plotted on the bottom x-axis.

DSC Dynamic Cooling Protocol

Step 1. The sperm cell suspension with or without cryoprotective agents (CPAs) initially at room temperature was cooled at 5°C/min until the extracellular ice nucleated.

Step 2. After nucleation the sample was thawed at a warming rate (5°C/min) such that phase-change temperature T_{ph} was reached (but not overshot) and ice remained in the extracellular solution. The phase change temperature can be obtained by using the osmolality relationship (Osm^{-1} = 1.858/ΔT; ΔT = 273.15 -T, K); thus, for a solution with an osmolality of 1000 mOsm, ΔT = 1.0*1.858 = ~1.858 K or T_{ph} = −1.858°C.

Step 3. The sample was cooled to −50°C at 5 (or 20)°C/min, allowing the sperm cells to undergo cellular dehydration. The lower curve in Figure 1 corresponds to the heat release associated with dehydration, and the total area is represented by $q_{initial}$.

Step 4. The sample was thawed at 20°C/min and re-equilibrated at T_{ph}.

Step 5. To differentiate between the heat released by the media and the intracellular fluid in Step 3, the sample was cooled at a high cooling rate (200°C/min) down to −150°C. This causes all the sperm cells to lyse and become osmotically inactive.

Step 6. Step 4 was repeated.

Step 7. The sample was cooled to −50°C at 5 (or 10)°C/min to measure the final heat release because of lysed or osmotically inactive sperm cells mixed with media. The upper curve in Figure 1 corresponds to this heat release, and the total area is represented by $q_{initial}$.

Translation of Heat Release to Cell Volume Data for Dynamic Cooling

The heat release measurements of interest are Δq_{dsc} and $\Delta q(T)_{dsc}$, which are the total and fractional difference between the heat releases measured by integration of the heat flows during freezing of osmotically active (live) cells in media and during freezing of osmotically inactive (dead) cells in media. This difference in heat release has been related to cell volume changes in several biological systems [27–33] as,

$$VT(T) = V_o - \frac{\Delta q(T)_{dsc}}{\Delta q_{dsc}}(V_o - V_b) \quad (1)$$

Note that the DSC-measured heat release readings $\Delta q(T)_{dsc}$ and Δq_{dsc} were obtained separately at 5°C/min (data not shown) and at 20°C/min (as shown in Fig. 1) in the absence and presence of dimethyl sulfoxide

TABLE 1. Measurements and calculated volumes, surface areas, and ratios of surface area to volume (S : V) for heads, tails, and combined totals of sperm from diploid and tetraploid Pacific oysters.

	Head				Tail					Total		
Ploidy	Diameter (μm)	Volume[a] (μm^3)	Surface[b] (μm^2)	S : V	Length (μm)	Width (μm)	Volume[c] (μm^3)	Surface[d] (μm^2)	S : V	Volume[e] (μm^3)	Surface[f] (μm^2)	S : V
Diploid	1.66	2.40	8.66	3.61	41	0.14	0.63	18.03	28.57	3.03	26.69	8.81
Tetraploid	2.14	5.13	14.39	2.81	53	0.17	1.20	28.31	23.53	6.33	42.69	6.74

[a] Calculated as volume of a sphere ($V_s = 4/3\pi R^3$).
[b] Calculated as surface area of sphere ($S_s = 4\pi R^2$).
[c] Calculated as volume of a cylinder ($V_c = \pi R^2 h$).
[d] Calculated as surface of a cylinder ($S_c = 2\pi Rh$).
[e] Calculated as sum of the volumes of the head and tail ($V_t = V_s + V_c$).
[f] Calculated as sum of the surface areas of the head and tail ($S_t = S_s + S_c$).

(DMSO). The unknowns needed in Equation (1) apart from the DSC heat release readings are V_o (the initial or the isotonic cell volume; in this study the oyster sperm cell is modeled as a "ball-on-stick" structure with the dimensions shown in Table 1 and Fig. 2) and V_b (the final osmotically inactive cell volume or 0.6 V_o; note that in the presence of 8% DMSO, this value increases to 0.626 V_o). The osmotically inactive cell volume, V_b, was assumed to be 0.6 V_o, a value within the range reported for a variety of mammalian sperm (because we are unaware of any published values of V_b of spermatozoa from any aquatic species) [36]. To further our understanding of the effect of V_b on the predicted oyster membrane permeability parameters and the model simulations, additional calculations were also performed assuming V_b = 0.8 V_o and 0.4 V_o.

Water Transport Model and Numerical Methods

Kedem and Katchalsky [37] proposed a model for water and solute transport in response to chemical potential gradients based on irreversible thermodynamics. If the flux of cryoprotective agent (CPA) is negligible in comparison to the water flux [38], then the Kedem-Katchalsky model reduces to a model that assumes only water transport, as proposed by Mazur [39] and later modified by Levin et al. [40] and Karlsson et al. [41]. The model predicts the change in cell volume with decreasing temperature (dV/dT) after ice has formed outside an unfrozen cell as

$$\frac{dV}{dT} = \frac{L_p A_c RT}{B}[C_i - C_o] \quad (2)$$

with L_p, the sperm cell membrane permeability to water defined by Levin et al. [40] as

$$L_p = L_{pg}[cpa]\exp\left(\frac{-E_{Lp}[cpa]}{R}\cdot\left(\frac{1}{T} - \frac{1}{T_R}\right)\right) \quad (3)$$

where, L_{pg} or $L_{pg}[cpa]$ is the reference membrane permeability at a reference temperature, T_R (= 273.15 K) in the absence and presence of CPA; E_{Lp} or $E_{Lp}[cpa]$ is the apparent activation energy (kJ/mol) or the temperature dependence of the cell membrane permeability in the absence and presence of CPA; A_c is the effective membrane surface area for water transport, assumed to be constant during the freezing process (see Table 1 and Fig. 2 for the geometric model of the oyster spermatozoa); R is the universal gas constant; B is the constant cooling rate K/min; finally C_i and C_o represent the concentrations of the intracellular and extracellular (unfrozen) solutions. The various assumptions made in the development of the water transport are discussed in detail elsewhere [33, 36–43] and are beyond the scope of the present study. The two unknown membrane permeability parameters of the model either $L_{pg}[cpa]$ and $E_{Lp}[cpa]$ in the presence of CPA or L_{pg} and E_{Lp} in the absence of CPA, are determined by curve fitting the water transport model to experimentally obtained volumetric shrinkage data during freezing.

Numerical Methods

A nonlinear least squares curve-fitting technique was implemented using a custom-written computer program to calculate the membrane permeability parameters that best fit the volumetric shrinkage data as previously described by Bevington and Robinson [44]. The optimal fit of Equation (2) to the experimental data was obtained by selecting a set of parameters that minimized the residual variance, chi-square, and maximized a goodness-of-fit parameter, R^2 [45]. To predict the membrane permeability parameters that produced a combined-best-fit to the experimental water transport data at two or more cooling rates, the nonlinear curve-fitting code was slightly modified such that R^2 was maximized by one set of parameters for all cooling rates as previously described [28–32, 43]. To simulate the biophysical response of a sperm cell under a variety of cooling rates, the best-fit parameters were substituted in the water transport equation, which was numerically solved using a fourth-order Runge-Kutta method using a FORTRAN code on a Mac Powerbook G4 (Apple Computer Inc., Cupertino, CA) workstation.

RESULTS

Dynamic Cooling Response and Membrane Permeability Parameters

Figure 3A shows the water transport data and simulation using best-fit parameters in Equation 3 at cooling rates of 5 and 20°C/min in the absence of CPAs for sperm cells of diploid Pacific oysters (or haploid sperm cells). The dynamic portion of the cooling curve is between −1.86°C and −8°C at these cooling rates. Water transport cessation is observed in the DSC heat release data as an overlap of the thermograms from the heat release signature obtained using osmotically active (initial) and inactive (final) cells, as seen in Figure 1. The best fit of Equation 3 to the 5°C/min diploid water transport data without DMSO was obtained for membrane permeability parameter values of $L_{pg} = 0.27 \times 10^{-15}$ m³/Ns (0.0015 μm/min-atm) and $E_{Lp} = 61.9$ kJ/mol (14.8 kcal/mol) were with an R^2 value of 0.99; whereas the corresponding values for the 20°C/min data: $L_{pg} = 0.36 \times 10^{-15}$ m³/Ns (0.0020 μm/min-atm) and $E_{Lp} = 41.8$ kJ/mol (10.0 kcal/mol) were with an R^2 value of 0.97 (Table 2). Similarly, Figure 3B shows the water transport data and simulation using the best-fit parameters in Equation 3 at cooling rates of 5 and 20°C/min in the presence of 8% (v/v) DMSO for haploid sperm cells. The dynamic portion of the cooling curve at these cooling rates is between −2.9°C and −11°C. The best-fit of Equation 3 to the 5°C/min water transport data in the presence of DMSO was obtained for membrane permeability parameter values of $L_{pg} = 0.23 \times 10^{-15}$ m³/Ns (0.0013 μm/min-atm) and $E_{Lp} = 51.4$ kJ/mol (12.3 kcal/mol) were with an R^2 value of 0.99, whereas the corresponding values for the 20°C/min data: $L_{pg} = 0.37 \times 10^{-15}$ m³/Ns (0.0021 μm/min-atm) and $E_{Lp} = 45.6$ kJ/mol (10.9 kcal/mol) were with an R^2 value of 0.97 (Table 2).

Figure 4, A and B, show the water transport data and simulation using best-fit parameters in Equation 3 at coolng rates of 5 and 20°C/min in the absence and presence of DMSO for sperm cells of tetraploid Pacific oysters (or diploid sperm cells), respectively. The dynamic portion of the cooling curve at these cooling rates was found to be between −1.86°C and −8°C in the absence of CPAs and between −2.9°C and −11°C in the presence of 8% (v/v) DMSO as shown in Figure 4, A and B, respectively. The best fit of Equation 3 to the 5°C/min tetraploid water trans-

port data without DMSO was obtained for membrane permeability parameter values of $L_{pg} = 0.27 \times 10^{-15}$ m^3/Ns (0.0015 μm/min-atm) and $E_{Lp} = 43.1$ kJ/mol (10.3 kcal/mol) were with an R^2 value of 0.99, whereas the corresponding values for the 20°C/min data: $L_{pg} = 0.50 \times 10^{-15}$ m^3/Ns (0.0028 μm/min-atm) and $E_{Lp} = 50.2$ kJ/mol (12.0 kcal/mol) were with an R^2 value of 0.96 (Table 2). Similarly, the best fit of Equation 3 to the 5°C/min diploid sperm water transport data with 8% DMSO was obtained for membrane permeability parameter values of $L_{pg} = 0.30 \times 10^{-15}$ m^3/Ns (0.0017 μm/min-atm) and $E_{Lp} = 43.1$ kJ/mol (10.3 kcal/mol) were with an R^2 value of 0.97, whereas the corresponding values for the 20°C/min data: $L_{pg} = 0.37 \times 10^{-15}$ m^3/Ns (0.0021 μm/min-atm) and $E_{Lp} = 41.4$ kJ/mol (9.9 kcal/mol) were with an R^2 value of 0.95 (Table 2).

Statistical Analysis

All of the curve-fitting results presented have an R^2 value greater than or equal to 0.95, indicating that there was a good agreement between the experimental data points and the fit calculated using the estimated membrane permeability parameters. The differences in the DSC water transport data at 5 and 20°C/min were found to be statistically significantly from one another with more than 95% confidence level (in the dynamic part of the cooling curve) in all the combinations investigated. And finally, the differences in the water transport data, when compared across concentrations of CPA (i.e., comparing the water transport data obtained with and without DMSO), were found to be statistically significant with a confidence level greater than 95% (at both 5 and 20°C/min).

Combined-Best-Fit Parameters

As stated earlier, a new set of membrane permeability parameters (L_{pg} and E_{Lp} or $L_{pg}[cpa]$ and $E_{Lp}[cpa]$) were obtained that produced a combined-best-fit to the experimentally determined water transport data (Table 2). The combined-best-fit membrane permeability parameters maximized the goodness-of-fit parameter, R^2, for the 5 and 20°C/min water transport data concurrently, as described in earlier studies [28–32, 43]. Figure 5 shows the contour plots of the goodness-of-fit parameter, R^2 (= 0.95) in the L_{pg} and E_{Lp} (or $L_{pg}[cpa]$ and $E_{Lp}[cpa]$) space that "fit" the water transport data at 5 and 20°C/min in the freezing media without CPAs for haploid sperm cells (Fig. 5A) and for diploid sperm cells (Fig. 5B). Similar contours are shown in Figure 5, C and D, for haploid and diploid oyster sperm cells in the presence of 8% DMSO. Any combination of L_{pg} and E_{Lp} (or $L_{pg}[cpa]$ and $E_{Lp}[cpa]$) shown to be within the contour will fit the water transport data at that cooling rate with an R^2 value of more than 0.95. Note that the contours for the higher cooling rate of 20°C/min were smaller than those obtained at the lower cooling rate of 5°C/min. This suggests that the membrane permeability parameters obtained using the 20°C/min water transport data would predict the volumetric response of the sperm cell at the lower cooling rate of 5°C/min accurately, whereas the converse was not true.

Water Transport Simulations

Water transport simulations obtained using the combined-best-fit parameters in Equation 3 are shown for a variety of cooling rates (5–100°C/min) in Figure 6. In Figure 6, A and B, the numerically simulated nondimensional cellular volume (V/V_o) obtained using the combined-best-fit parameters is shown for a variety of cooling rates (5, 20, 40, 50, and 100°C/min) in the absence of CPAs for sperm cells from diploid and tetraploid Pacific oysters. Similar simulations are shown in Figure 6, C and D, for sperm cells from diploid and tetraploid Pacific oysters in the presence of 8% DMSO. The nondimensional cellular volume (V/V_o), which decreases because of dehydration during freezing, is plotted on the y-axis, whereas the subzero temperatures are plotted on the x-axis. From the simulations, the amount of

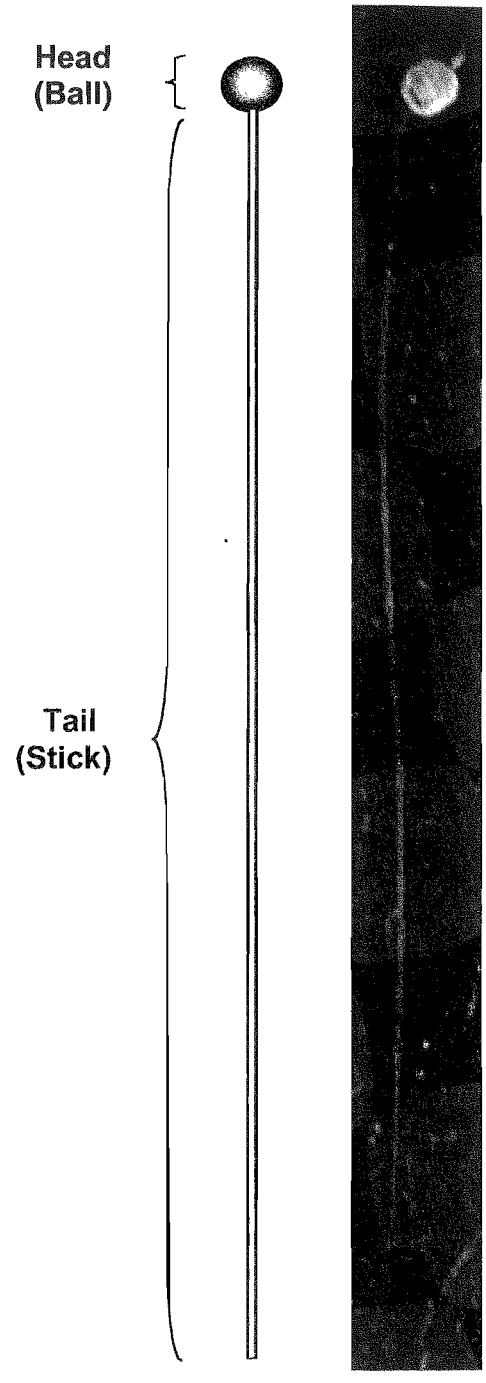

FIG. 2. **Left)** "Ball-on-stick" model used to calculate the sperm cell volumes and surface areas from diploid and tetraploid Pacific oysters. **Right)** Representative scanning electron micrographs (SEM) of sperm from tetraploid Pacific oysters showing the relationship of sperm head and tail in alignment with model used to calculate the cell volumes and surface areas shown in Table 1.

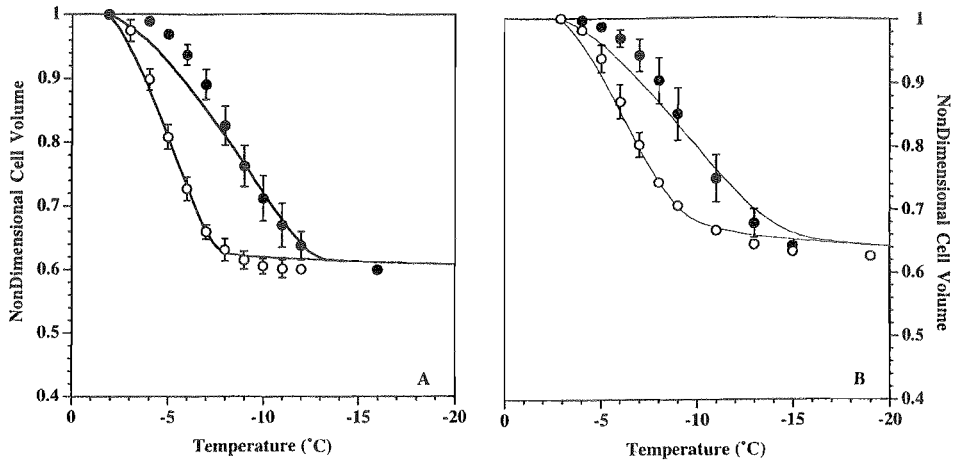

FIG. 3. Volumetric response of haploid sperm cells (or cells from diploid Pacific oysters) as a function of subzero temperatures obtained using the DSC technique in the presence of extracellular ice in the absence of CPAs (A) and the presence of extracellular ice and DMSO (B). The open and filled circles represent the DSC water transport (volumetric shrinkage) data at the cooling rate of 5 and 20°C/min. The dynamic cooling response at 5 and 20°C/min is shown as a solid line and was obtained by using the best-fit membrane permeability parameters (L_{pg} and E_{Lp} or $L_{pg}[cpa]$ and $E_{Lp}[cpa]$) (Table 2) in the water transport equation (Equations 3 and 4). The nondimensional cell volume is plotted along the y-axis and the subzero temperatures are shown along the x-axis. The error bars represent the SD for the mean values of six DSC experiments.

trapped water (or a lower boundary on the intracellular ice) was computed as a ratio of the volume of the water trapped inside the sperm cell at the temperature, T (~−30°C) in which intracellular ice formation can occur by a homogenous or volume-catalyzed nucleation [46] to the initial sperm water volume, $[(V-V_b)/(V_o-V_b)]$ (where V is the end volume after water transport ceases [at ~−30°C], and V_o and V_b are the initial [isotonic] and final [osmotically inactive] sperm cell volumes) as described earlier for a several biological systems [28–32, 33, 43].

For haploid sperm cells (or cells from diploid Pacific oysters) in the absence of CPAs, for cooling rates of less than or equal to 40, 50, and 100°C/min, the trapped water volume was less than or equal to 1.25%, 1.75%, and 47.25% of the initial osmotically active water volume, and the end volumes were less than or equal to 0.605 V_o, 0.607 V_o and 0.789 V_o (Fig. 6A). For haploid sperm cells, in the presence of 8% DMSO, for cooling rates of less than or equal to 20, 40, 50, and 100°C/min, the trapped water volume was less than or equal to 1.60%, 2.41%, 11.50%, and 52.41% of the initial osmotically active water volume, and the end volumes were less than or equal to 0.632 V_o, 0.635 V_o, 0.669 V_o, and 0.822 V_o (Fig. 6C). Similarly, for diploid sperm cells (or cells from tetraploid Pacific oysters) in the absence of CPAs, for cooling rates of less than or equal to 50 and 100°C/min, the trapped water volume was less than or equal to 1.25% and 37.5% of the initial osmotically active water volume, and the end volumes were less than or equal to 0.605 V_o and 0.75 V_o (Fig. 6B). And finally, for diploid sperm cells in the presence of 8% DMSO, for cooling rates of less than or equal to 20, 40, 50, and 100°C/min, the trapped water volume was less than or equal to 1.60%, 2.41%, 12.30%, and 52.94% of the initial osmotically active water volume, whereas the end volumes were less than or equal to 0.632 V_o, 0.635 V_o, 0.672 V_o, and 0.824 V_o, respectively (Fig. 6D).

As stated in the *Introduction*, the cooling rate that optimizes cell survival after a freeze thaw for any cellular system can be defined as the fastest cooling rate in a given media without forming damaging IIF [5]. Mazur [47] defines IIF as damaging and lethal if 10–15% of the initial intracellular water is involved. We defined the *optimal cooling rate* as the cooling rate at which 5% of the initial osmotically active water volume was trapped inside the cells at −30°C. Note that if IIF occurs by a heterogeneous or a surface-catalyzed nucleation mechanism [46] (generally between −5 and −20°C for a variety of single cells), which our model does not predict, then potentially even more water would be trapped in the sperm cells than predicted by water transport alone (i.e., the lower boundary of intracellular ice discussed above). Thus, the optimal cooling rates based on the lower boundary of intracellular ice would be overestimated. Based on the simulations (shown in Fig. 6) obtained using the combined-best-fit parameters, the optimal cooling rate in the absence and presence of a CPA for haploid sperm cells were ~53°C/min and ~44°C/min. Sim-

TABLE 2. Predicted subzero membrane permeability parameters for Pacific oyster sperm cells in the presence and absence of DMSO assuming $V_b = 0.6V_o$.

Pacific oyster type (sperm cell)	Conc. of DMSO (v/v)	Cooling rate (°C/min)	L_{pg} or $L_{pg}[cpa]$ $\times 10^{15}$ m³/Ns (μm/min-atm)	E_{Lp} or $E_{Lp}[cpa]$ kJ/mol (kcal/mol)	R^2 value
Diploid (Haploid)	0%	5	0.27 (0.0015)	61.9 (14.8)	0.99
	(No CPA)	20	0.36 (0.0020)	41.8 (10.0)	0.97
		CBF[a]	0.30 (0.0017)	41.0 (9.8)	0.96
	8%	5	0.23 (0.0013)	51.4 (12.3)	0.99
		20	0.37 (0.0021)	45.6 (10.9)	0.97
		CBF[a]	0.27 (0.0015)	38.0 (9.1)	0.96
Tetraploid (Diploid)	0%	5	0.27 (0.0015)	43.1 (10.3)	0.99
	(No CPA)	20	0.50 (0.0028)	50.2 (12.0)	0.96
		CBF[a]	0.34 (0.0019)	29.7 (7.1)	0.95
	8%	5	0.30 (0.0017)	43.1 (10.3)	0.97
		20	0.37 (0.0021)	41.4 (9.9)	0.95
		CBF[a]	0.34 (0.0019)	37.6 (9.0)	0.96

[a] The combined-best-fit (CBF) parameters maximized the R^2 value, concurrently, at both 5 and 20°C/min.

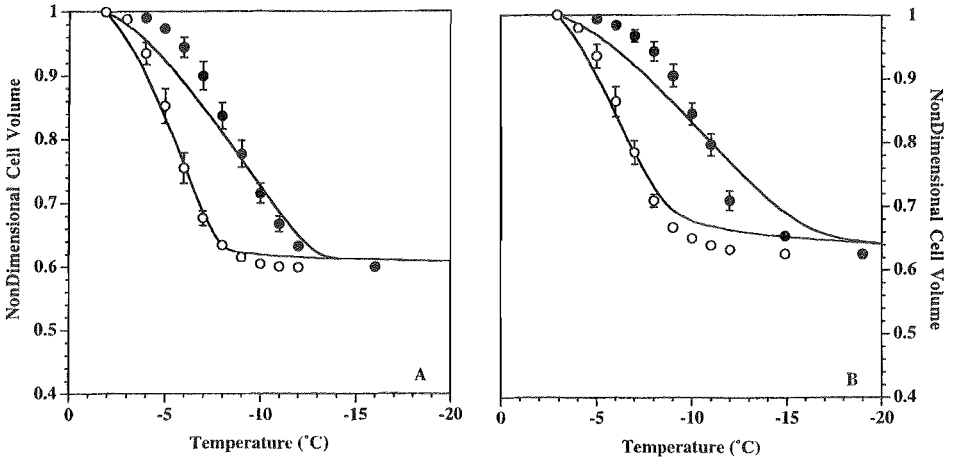

FIG. 4. Volumetric response of diploid sperm cells (or cells from tetraploid Pacific oysters) as a function of subzero temperatures obtained using the DSC technique in the presence of extracellular ice but in the absence of CPAs (**A**) and in the presence of extracellular ice and DMSO (**B**). The open and filled circles represent the DSC water transport (volumetric shrinkage) data at the cooling rate of 5 and 20°C/min. The model-simulated dynamic cooling response at 5 and 20°C/min is shown as a solid line and was obtained by using the best-fit membrane permeability parameters (L_{pg} and E_{Lp} or $L_{pg}[cpa]$ and $E_{Lp}[cpa]$) (Table 2) in the water transport equation (Equations 3 and 4). The nondimensional volume is plotted along the y-axis and the subzero temperatures are shown along the x-axis. The error bars represent the SD for the mean values of six DSC experiments.

ilarly, the optimal cooling rates in the absence and presence of a CPA for diploid sperm cells were ~63°C/min and ~43°C/min.

Parameter Sensitivity Analysis—Effect of Varying the Osmotically Inactive Cell Volume (V_b)

The value of the osmotically inactive cell volume of mammalian sperm cells has been reported to range from 0.6 V_o (the value used in this and other studies) to as low as 0.25 V_o and as high as 0.80 V_o [28–33, 36]. To study the effect of varying the osmotically inactive cell volume on the predicted membrane permeability parameters (L_{pg} and E_{Lp} or $L_{pg}[cpa]$ and $E_{Lp}[cpa]$), the value of V_b was increased to 0.8 V_o and decreased to 0.4 V_o. The DSC data were correspondingly modified (using Equation 1), and the modified data were fitted to the water transport model (Equations 2 and 3) using the nonlinear least squares curve-fitting technique as previously described. The predicted values of the membrane permeability parameters using an osmotically inactive cell volume of 0.4 V_o and 0.8 V_o were then obtained both in the presence and absence of DMSO (data not shown in the interest of brevity). The predicted optimal cooling rates obtained using these parameters were in good agreement (± 10%) to the values obtained with V_b of 0.6 V_o described earlier. Thus, the variation in the value of V_b did not significantly alter the model predictions, and as noted earlier depending on the concentration of DMSO, cooling rates as low as 40–70°C/min can cause a significant volume of intracellular water to be trapped inside the oyster spermatozoa.

Parameter Sensitivity Analysis—Effect of Varying the Cell Geometry

To study the effect of varying the cell membrane surface (A_c) and cell volume (V_o) on the predicted membrane permeability parameters (L_{pg} and E_{Lp} or $L_{pg}[cpa]$ and $E_{Lp}[cpa]$), it was assumed that the oyster sperm cells could be modeled as isolated spherical cells or as heads alone (with diameters of 1.66 and 2.14 μm for haploid and diploid sperm cells; see Table 1). The corresponding membrane permeability parameters (L_{pg} and E_{Lp} or $L_{pg}[cpa]$ and $E_{Lp}[cpa]$) are shown in Table 3. Additional numerical simulations were performed assuming a spherical model for the oyster sperm cells and using the combined-best-fit parameters (Table 3) in the water transport model (Equations 2 and 3). As before, an analysis of these simulations was performed to predict the lower boundary on trapped intracellular ice and the optimal rate of freezing oyster sperm cells. The predicted optimal cooling rates of haploid sperm cells in the absence and presence of 8% DMSO, assuming a spherical model were ~62°C/min and ~47°C/min. Similarly, the optimal cooling rates in the absence and presence of DMSO, for diploid oyster sperm cells were ~42°C/min and ~39°C/min. These optimal cooling rate values are in the same range as those obtained with the "ball-on-stick" model, presented earlier.

DISCUSSION

Independent verification of the predicted optimal cooling rates is obtained by comparing the experimentally determined optimal rates of freezing reported in the literature for Pacific oyster sperm cells [15–19] and other oyster sperm cells [20–23]. In general, Pacific oyster sperm cells are found to exhibit the highest postthaw function (cell viability and relative larval yield) when cooled at 40–80°C/min in the presence of 8% (v/v) DMSO [17]. However, further empirical studies are needed to corroborate the predicted optimal rates of freezing haploid and diploid Pacific oyster sperm cells reported in the present study.

Effect of Varying the Cell Geometry

The reference membrane permeability (L_{pg} or $L_{pg}[cpa]$) values obtained using the spherical cell (heads alone) model (Table 3) are uniformly higher than those obtained using the "ball-on-stick" (head and tail) model (Table 2). This increase in the predicted membrane permeability between the "ball-on-stick" and the spherical cell model is not surprising because Equation 2 shows that the change in the oyster sperm cell volume as a function of temperature (dV/dT) is proportional to the product of L_p and A_c. Note that the spherical cell model has lower surface area available for water transport than the "ball-on-stick" model (Table 1). Thus, for a given change in the oyster sperm cell volume as a function of temperature (dV/dT), a decrease in A_c will cause a corresponding increase in the predicted value of L_p or $L_p[cpa]$ where $L_p = f(L_{pg}, E_{Lp})$ and $L_p[cpa] = f(L_{pg}[cpa], E_{Lp}[cpa])$. Thus, any changes to the geometrical model of the oyster sperm cell (specifically membrane surface area, A_c and isotonic cell volume, V_o) should manifest themselves with corresponding changes to the model pre-

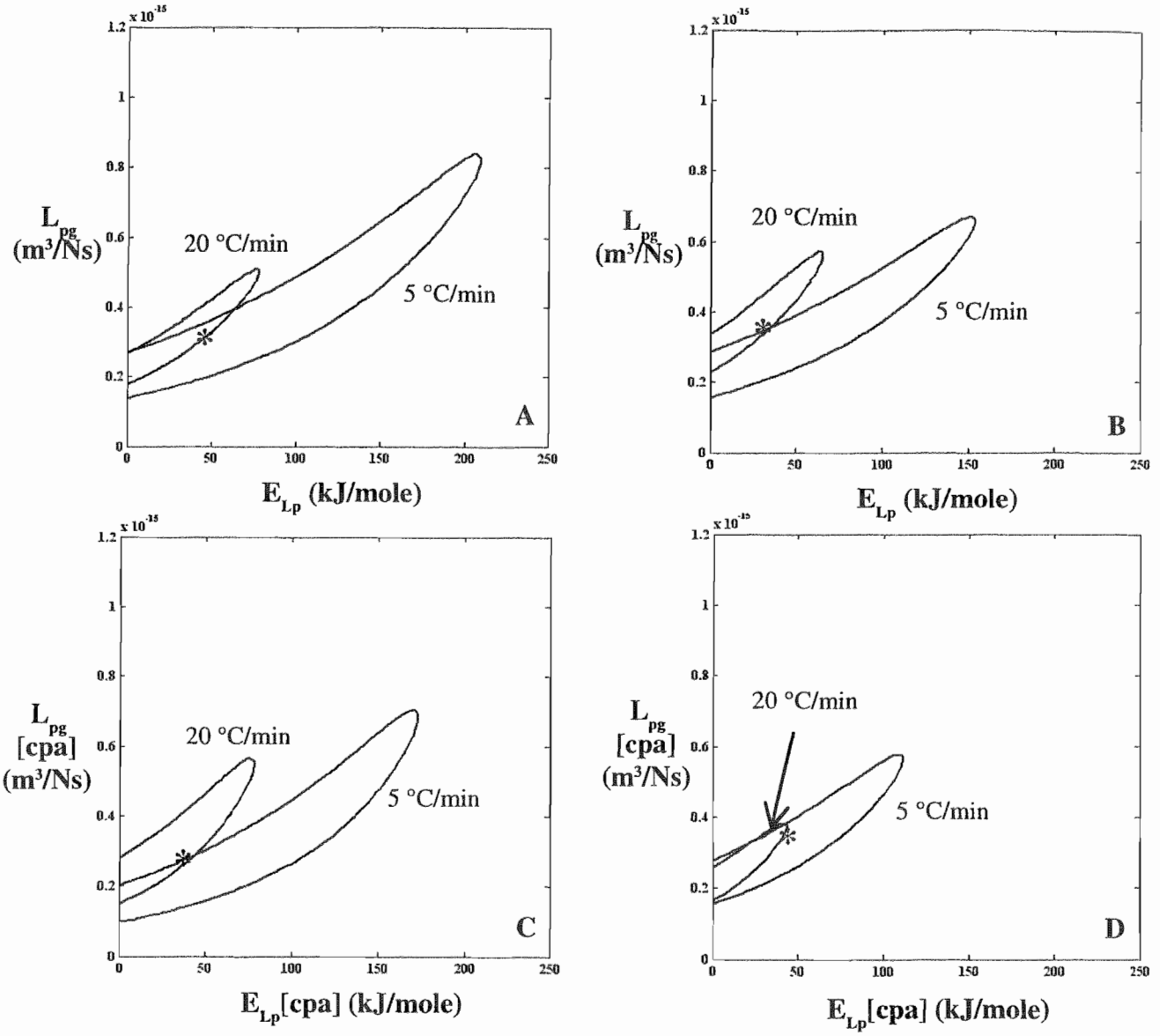

FIG. 5. Contour plots of the goodness-of-fit parameter R^2 (= 0.95) for water transport response in Pacific oyster sperm cells in the presence and absence of DMSO. The common region corresponds to the range of parameters that fit the water transport data at two cooling rates (5 or 20°C/min) with R^2 of 0.95 or more. Asterisks represent the combined-best-fit parameters in all the panels. The membrane permeability at 0°C, L_{pg} (or $L_{pg}[cpa]$; m³/Ns) is plotted on the y-axis whereas the apparent activation energy of the membrane, E_{Lp} (or $E_{Lp}[cpa]$; kJ/mol) is plotted on the x-axis. **A**) Haploid sperm cells without DMSO: the combined-best-fit parameters were: L_{pg} = 0.30 × 10 $^{-15}$ m³/Ns (0.0017 μm/min-atm) and E_{Lp} = 41.0 kJ/mol (9.8 kcal/mol). **B**) Diploid sperm cells without DMSO: the combined-best-fit parameters were: L_{pg} = 0.34 × 10 ^{15} m³/Ns (0.0019 μm/min-atm) and E_{Lp} = 29.7 kJ/mol (7.1 kcal/mol). **C**) Haploid sperm cells with DMSO: the combined-best-fit parameters were: L_{pg} = 0.27 × 10^{-15} m³/Ns (0.0015 μm/min-atm) and E_{Lp} = 38.0 kJ/mol (9.1 kcal/mol). **D**) Diploid sperm cells with DMSO: the combined-best-fit parameters were: L_{pg} = 0.34 × 10^{-15} m³/Ns (0.0019 μm/min-atm) and E_{Lp} = 37.6 kJ/mol (9.0 kcal/mol).

dicted membrane permeability parameters (L_{pg} and E_{Lp} or $L_{pg}[cpa]$ and $E_{Lp}[cpa]$) [48].

Effect of Cooling Rate on Predicted Membrane Permeability Parameters

There was good agreement (±20%) in the predicted value of the activation energy, E_{Lp} (or $E_{Lp}[cpa]$) at 5 and 20°C/min for haploid and diploid sperm cells in the absence and presence of DMSO (with the exception of diploid sperm cells with an assumed V_b of 0.8 V_o). This lack of variation in the activation energy values between 5 and 20°C/min suggests that the oyster sperm cells cooled at 20°C/min underwent complete dehydration, and the final end volume was comparable with the assumed value of the osmotically inactive cell volume. This assertion is further supported by the observations that: 1) the magnitude of the DSC-measured difference in heat release, Δq_{dsc}, was found to be constant between 5 and 20°C/min; and 2) no secondary heat release was observed at 20°C/min, suggesting incomplete dehydration, as was the case for Epstein Barr virus-transformed lymphocytes [27] and liver tissue of a freeze-tolerant wood frog, *Rana sylvatica* [49]. As stated in earlier studies [27–33], a major disadvantage of the DSC technique is its inability to distinguish heat released because of water transport and IIF. Based on our results, it is reasonable to presume that oyster sperm cells cooled at 20°C/min did in fact undergo complete dehydration (in which water transport was the dominant biophysical mechanism), and hence the DSC results at the higher cooling rate of 20°C/min were

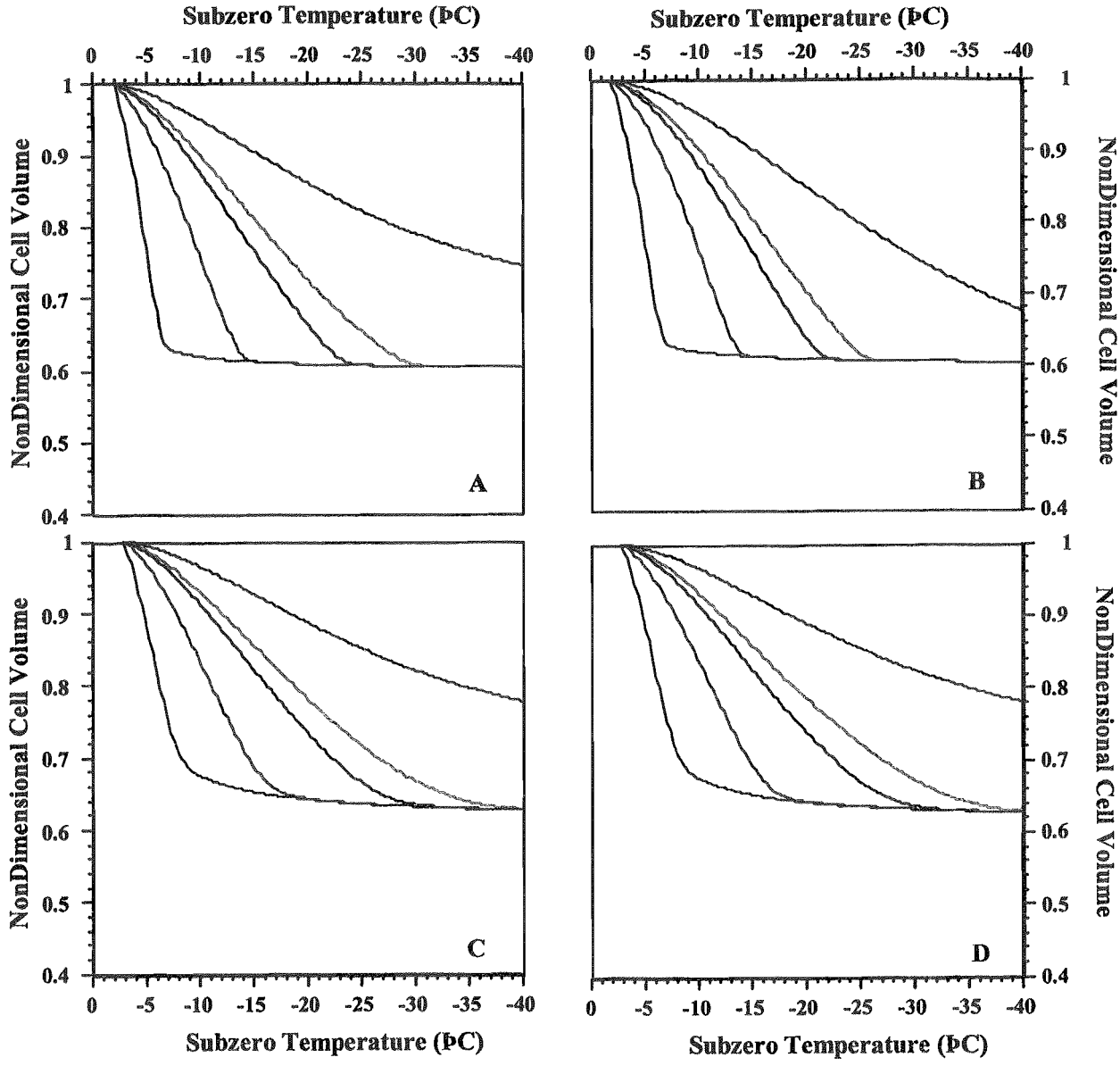

FIG. 6. Volumetric response of Pacific oyster sperm cells at various cooling rates as a function of subzero temperature using the combined-best-fit membrane permeability parameters (Table 2). **A–D**) The changes in the normalized cell volume (V/V_o) are shown as a function of temperature for different cooling rates in haploid sperm cell suspensions without DMSO (**A**), diploid sperm cell suspensions without DMSO (**B**), haploid sperm cell suspensions without DMSO (**C**), and diploid sperm cell suspensions with DMSO (**D**). The water transport curves represent the model-simulated response for different cooling rates (from left to right: 5, 20, 40, 50, and 100°C/min). The subzero temperatures are shown along the x-axis, whereas the nondimensional volume is plotted along the y-axis.

indicative of the rate of cellular water loss from oyster sperm cells.

Effect of CPAs on Membrane Transport Parameters

The DSC technique was used to obtain water transport data and water permeability parameters ($L_{pg}[cpa]$ and $E_{Lp}[cpa]$) of oyster sperm cells in the presence of DMSO. Although the exact mechanism by which the presence of DMSO or other CPAs modifies the water permeability parameters is as yet unknown, several studies have shown that the presence of CPAs tends to reduce the membrane permeability parameters, $L_{pg}[cpa]$ and $E_{Lp}[cpa]$ [28–33, 43, 50]. This is at least partially the case in the present study, in which an increase in the concentration of solutes in the extracellular medium was shown to reduce, although not significantly, the predicted value of membrane permeability parameters for Pacific oyster sperm cells. However, the addition of DMSO actually resulted in an increase in the predicted values of the "combined best-fit" membrane permeability parameters for diploid sperm cells. Further studies are clearly needed to elucidate the mechanism by which CPAs modify membrane permeability parameters.

Effect of Oyster Cell Type on Membrane Transport Parameters

As stated earlier, the differences in the measured water transport data between haploid and diploid oyster sperm cells were not statistically significant. It is possible that the DSC technique cannot distinguish the "subtle" differences in water transport between these cells. This possibility is small, given a recent study on equine sperm that demonstrated differences in volumetric shrinkage among samples

TABLE 3. Predicted subzero membrane permeability parameters for Pacific oyster sperm cells: neglecting the sperm cell tail volume and surface area and modeling the sperm cell heads as spheres with dimensions shown in Table 1 and $V_b = 0.6V_o$.

Pacific oyster type (sperm cell)	Conc. of DMSO (v/v)	Cooling rate (°C/min)	L_{pg} or $L_{pg}[cpa]$ $\times 10^{15}$ m³/Ns (μm/min-atm)	E_{Lp} or $E_{lp}[cpa]$ kJ/mol (kcal/mol)	R^2 value
Diploid (Haploid)	0%	5	0.75 (0.0042)	79.8 (19.1)	0.99
	(No CPA)	20	0.82 (0.0046)	38.0 (9.1)	0.98
		CBF[a]	0.71 (0.0040)	34.7 (8.3)	0.97
	8%	5	0.52 (0.0029)	47.7 (11.4)	0.99
		20	0.78 (0.0044)	34.3 (8.2)	0.98
		CBF[a]	0.71 (0.0040)	39.3 (9.4)	0.96
Tetraploid (Diploid)	0%	5	0.68 (0.0036)	44.7 (10.7)	0.99
	(No CPA)	20	1.07 (0.0060)	41.8 (10.0)	0.97
		CBF[a]	0.71 (0.0040)	39.3 (9.4)	0.96
	8%	5	0.73 (0.0041)	38.9 (9.3)	0.97
		20	0.80 (0.0045)	33.4 (8.0)	0.96
		CBF[a]	0.85 (0.0048)	43.2 (10.3)	0.96

[a] The combined-best-fit (CBF) parameters maximized the R^2 value, concurrently, at both 5 and 20°C/min.

that were collected and cooled to 4°C under different conditions, including osmotic shock and cold shock [51]. Thus, it is likely that the ability of oyster sperm cells to shrink in the presence of extracellular ice during a thermal insult is independent of the ploidy level. However, differences in the size of the sperm cells did result in different membrane permeability parameters for haploid and diploid oyster sperm cells. Cursory evaluation of the predicted membrane permeability parameters did not determine any consistent effect of cell type on the predicted parameters (L_{pg} and E_{Lp} or $L_{pg}[cpa]$ and $E_{Lp}[cpa]$). Also, an examination of the contour plots shown in Figure 5 suggested that the parametric space that would "fit" the haploid sperm cell water transport data is significantly larger than that for diploid sperm cells (comparing the contours of Fig. 5A with Fig. 5B, especially at 5°C/min in the absence of DMSO; and the contours of Fig. 5C with that of Fig. 5D, especially at 20°C/min in the presence of DMSO). This suggests that the membrane permeability parameters obtained for the diploid sperm cells would predict the volumetric response of the haploid sperm cell quite accurately, whereas the converse was not true. Further illustration of this observation was obtained by comparing the predicted optimal cooling rates with diploid sperm cell parameters and the haploid sperm cell volume and surface area with those obtained earlier with haploid cell parameters and haploid cell dimensions (41 vs. 53°C/min in the absence of DMSO and 34 vs. 44°C/min with DMSO or ± 22% of each other). Conversely, the predicted optimal cooling rates with haploid sperm cell parameters and the diploid cell volume and surface area with those obtained earlier with diploid cell parameters and diploid cell dimensions were significantly different (83 vs. 63°C/min in the absence of DMSO and 57 vs. 43°C/min with DMSO or ± 33% of each other). It is as yet unclear whether this is a general effect related to the ploidy level of the sperm cells or a unique result for sperm cells from diploid and tetraploid Pacific oysters, *C. gigas*.

In summary, water transport (volumetric shrinkage) was evaluated for haploid and diploid oyster sperm cells in the presence of extracellular ice and a CPA (DMSO) during freezing using the DSC technique at two different cooling rates (5 and 20°C/min). This represents the first such effort for sperm cells from any aquatic species. The predicted "combined best-fit" permeability parameters ranged from L_{pg} or $L_{pg}[cpa] = 0.23 \times 10^{-15}$ to 0.50×10^{-15} m³/Ns (0.0013 to 0.0028 μm/min-atm) and E_{Lp} or $E_{Lp}[cpa] = 37.6$ to 61.9 kJ/mol (9.0 to 14.8 kcal/mol), whereas the predicted optimal rates of freezing ranged from 40 to 70°C/min. It is hoped that the water permeability parameters presented in this study will help to establish cryopreservation of Pacific oyster sperm cells on a firm biophysical basis. Future studies should make direct comparisons of the optimal cooling rates predicted using the water transport models developed here with empirical values for spermatozoa of Pacific oysters, *C. gigas*.

REFERENCES

1. Mazur P. Cryobiology: the freezing of biological systems. Science 1970; 168:939–949.
2. Meryman HT. Review of biological freezing. In: Meryman HT (ed.), Cryobiology. New York: Academic Press; 1966.
3. Mazur P. Freezing of living cells: mechanisms and implications. Am J Phys 1984; 247:C125–C142.
4. Lovelock JE. Haemolysis of human red blood-cells by freezing and thawing. Biochim Biophys Acta 1953; 10:414–426.
5. Mazur P, Leibo SP, Chu EHY. A two-factor hypothesis of freezing injury. Exp Cell Res 1972; 71:345–355.
6. Tiersch TR. Introduction. In: Tiersch TR, Maxik PM (eds.), Cryopreservation in Aquatic Species. Baton Rouge, LA: World Aquaculture Society; 2000: xix–xxvi.
7. Tiersch TR, Maxik PM. Cryopreservation in Aquatic Species. In: Tiersch TR, Maxik PM (eds.), Baton Rouge, LA: World Aquaculture Society; 2000.
8. Smith JF, Pugh PA, Tervit HR, Roberts RD, Janke AR, Kaspar HF, Adams SL. Cryopreservation of shellfish sperm, eggs and embryos. In: Proceedings of the New Zealand Society of Animal Production; 2001; 61:31–34.
9. Lin TT, Lung K. IIF characteristics of oyster embryos and eggs determined by a feedback controlled directional cryomicroscope. Cryobiology 1995; 32:566.
10. Zhang T, Rawson DM. Permeability of the vitelline membrane of zebrafish (*Brachydanio rerio*) embryos to methanol and propane-1, 2-diol. Cryo Lett 1996; 17:273–280.
11. Hagedorn M, Hsu E, Pilatus U, Wildt DE, Rall WF, Blackband SJ. Magnetic resonance microscopy and spectroscopy reveal kinetics of cryoprotectant permeation in a multicompartmental biological system. In: Proceedings of the National Academy of Sciences 1996; 93:7454–7459.
12. Blaxter JHS. Sperm storage and cross-fertilization of spring and autumn spawning herring. Nature 1953; 172:1189–1190.
13. Rana KJ. Cryopreservation of fish spermatozoa: cryopreservation and freeze-drying protocols. Methods Mol Biol 1995; 38:151–165.
14. Tiersch TR. Cryopreservation in aquarium fishes. Mar Biotechnol 2001; 3:212–223.
15. Lannan JE. Experimental self-fertilization of the Pacific oyster, *Crassostrea gigas*, utilizing cryopreserved sperm. Genetics 1971; 68:599–601.

16. Staeger WH. Cryobiological investigation of the gametes of the Pacific oyster *Crassostrea gigas*. Corvallis, OR: Oregon State University; 1973. Thesis.
17. Usuki H, Hamaguchi M, Ishioka H. Long-term cryopreservation of Pacific oyster *Crassostrea gigas* sperm. Bull Nansei Natl Fish Res Inst 1997; 30:115–123.
18. Kurokura H, Namba K, Ishikawa T. Lesions of spermatozoa by cryopreservation in oyster *Crassostrea gigas*. Bull Japan Soc Sci Fish 1990; 56:1803–1806.
19. Dong Q, Eudeline B, Allen S, Tiersch TR. Factors affecting sperm motility of tetroploid Pacific oysters. J Shellfish Res 2002; 21:719–723.
20. Paniagua-Chavez CG, Tiersch TR. Laboratory studies of cryopreservation of sperm and trochophore larvae of the eastern oyster. Cryobiology 2001; 43:211–223.
21. Hughes JB. An examination of eggs challenged with cryopreserved spermatozoa of the American oyster, *Crassostrea virginica*. Cryobiology 1973; 10:342–344.
22. Zell SR, Bamford MH, Hidu H. Cryopreservation of spermatozoa of the American oyster *Crassostrea virginica* Gmelin. Cryobiology 1979; 16:448–460.
23. Yankson K, Moyse J. Cryopreservation of the spermatozoa of *Crassostrea tulipa* and three other oysters. Aquaculture 1991; 97:259–267.
24. Allen SK, Downing SL. Consumers and "experts" alike prefer the taste of sterile triploid over gravid diploid Pacific oysters (*Crassostrea gigas*, Thunburg, 1793). J Shellfish Res 1991; 10:19–22.
25. Akashige S, Fushimi T. Growth, survival, and glycogen content of triploid Pacific oyster *Crassostrea gigas* in the waters of Hiroshima, Japan. Nippon Suisan Gakkaishi 1992; 58:1063–1071.
26. Allen SK, Bushek D. Large scale production of triploid *Crassostrea virginica* (Gmelin) using "stripped" gametes. Aquaculture 1992; 103: 241–251.
27. Devireddy RV, Raha D, Bischof JC. Measurement of water transport during freezing in cell suspensions using a differential scanning calorimeter. Cryobiology 1998; 36:124–155.
28. Devireddy RV, Swanlund DJ, Roberts KP, Bischof JC. Sub-zero water permeability parameters of mouse spermatozoa in the presence of extracellular ice and cryoprotective agents. Biol Reprod 1999; 61:764–775.
29. Devireddy RV, Swanlund DJ, Roberts KP, Pryor JL, Bischof JC. The effect of extracellular ice and cryoprotective agents on the water permeability parameters of human sperm plasma membrane during freezing. Hum Reprod 2000; 15:1125–1135.
30. Devireddy RV, Olin T, Swanlund DJ, Vincente W, Troedsson MHT, Bischof JC, Roberts KP. Cryopreservation of equine spermatozoa: optimal cooling rates in the presence and absence of cryoprotective agents. Biol Reprod 2002; 66:222–231.
31. Thirumala S, Ferrer MS, Al-Jarrah A, Eilts BE, Paccamonti DL, Devireddy RV. Cryopreservation of canine spermatozoa: theoretical prediction of optimal cooling rates in the presence and absence of cryoprotective agents. Cryobiology 2003; 47:109–124.
32. Devireddy RV, Fahrig B, Godke RA, Leibo SP. Subzero water transport characteristics of boar spermatozoa confirm observed optimal cooling rates. Mol Reprod Dev 2004; 67:446–457.
33. Devireddy RV, Bischof JC. Recent advances in cryobiology using calorimetry. In: Kakac S, Smirnov H, Mila MR (eds.), Low Temperature and Cryogenic Refrigeration. Dordrecht, The Netherlands: Kluwer Academic Publishers; 2003:265–294.
34. Yuan S, Diller KR. Study of freezing biological systems using optical differential scanning calorimeter. ASME summer BED conference proceedings 2001; 50:117–118.
35. Diller KR. New techniques in cryomicroscopy. Cryobiology 2002; 45: 250–251.
36. Gao DY, Mazur P, Critser JK. Fundamental cryobiology of mammalian spermatozoa. In: Karow AM, Critser JK (eds.), Reproductive Tissue Banking. San Diego, CA: Academic Press; 1997:263–328.
37. Kedem O, Katchalsky A. Thermodynamic analysis of the permeability of biological membranes to non-electrolytes. Biochim Biophys Acta 1958; 27:229–246.
38. McCaa C, Diller KR, Aggarawal SJ, Takahashi T. Cryomicroscopic determination of the membrane osmotic properties of human monocytes at subfreezing temperatures. Cryobiology 1991; 28:391–399.
39. Mazur P. Kinetics of water loss from cells at subzero temperatures and the likelihood of intracellular freezing. J Gen Physiol 1963; 47: 347–369.
40. Levin RL, Cravalho EG, Huggins CG. A membrane model describing the effect of temperature on the water conductivity of erythrocyte membranes at subzero temperatures. Cryobiology 1976; 13:415–429.
41. Karlsson JO, Cravalho EG, Toner M. A model of diffusion-limited ice growth inside biological cells during freezing. J Appl Physiol 1994; 75:4442–4455.
42. McGrath JJ. Membrane transport properties. In: McGrath JJ, Diller KR (eds.), Low Temperature Biotechnology: Emerging Applications and Engineering Contributions, BED-vol. 10, HTD-vol. 98. New York: ASME Press; 1988:273–330.
43. Smith DJ, Schulte M, Bischof JC. The effect of dimethylsulfoxide on the water transport response of rat hepatocytes during freezing. ASME J Biomech Eng 1998; 120:549–558.
44. Bevington PR, Robinson DK. Data Reduction and Error Analysis for the Physical Sciences, 2nd ed. New York: McGraw-Hill; 1992.
45. Montgomery DC, Runger GC. Applied Statistics and Probability for Engineers. New York: John Wiley & Sons; 1994:471–529.
46. Toner M. Nucleation of ice crystals in biological cells. In: Steponkus PL (ed.), Advances in Low-Temperature Biology, vol. 2. Greenwich, CT: JAI Press; 1993:1–52.
47. Mazur P. Equilibrium, quasi-equilibrium, and nonequilibrium freezing of mammalian embryos. Cell Biophys 1990; 17:53–92.
48. Devireddy RV, Smith DJ, Bischof JC. Mass transfer during freezing in rat prostate tumor tissue. Am Inst Chem Eng J 1999; 45:639–654.
49. Devireddy RV, Barratt PR, Storey KB, Bischof JC. Liver freezing response of the freeze-tolerant wood frog, *Rana sylvatica*, in the presence and absence of glucose. I Experimental measurements. Cryobiology 1999; 38:310–326.
50. Gilmore JA, McGann LE, Liu J, Gao DY, Peter AT, Kleinhans FW, Critser JK. Effect of cryoprotectant solutes on water permeability of human spermatozoa. Biol. Reprod 1995; 53:985–995.
51. Devireddy RV, Swanlund DJ, Alghamdi AS, Duoos LA, Troedsson MHT, Bischof JC, Roberts KP. Measured effect of collection and cooling conditions on the motility and the water transport parameters at subzero temperatures of equine spermatozoa. Reprod 2002; 124:643–648.